J. Fluid Mech. (2004), *vol.* 503, *pp.* 321–343.
DOI: 10.1017/S002211200400792X Printed in the United Kingdom

Long wave forcing on a barred beach

By T. E. BALDOCK[1], T. J. O'HARE[2] AND D. A. HUNTLEY[2]

[1]Department of Civil Engineering, University of Queensland, St Lucia, Brisbane, Qld 4072, Australia

[2]School of Earth, Ocean and Environmental Sciences, University of Plymouth, Drake Circus, Plymouth PL4 8AA, UK

(Received 26 February 2003 and in revised form 29 September 2003)

We present new laboratory data on long wave forcing over a barred beach profile under random wave breaking conditions. The data include incident and radiated wave amplitudes, wave set-up, and detailed measurements of the cross-shore variation in long wave amplitude, including shoreline (swash) amplitudes. The total surf zone width was varied via changes in both wave height and the water level over the bar crest. The data obtained from the barred beach are also compared with previous data obtained from a plane beach under essentially identical short wave forcing conditions. The presence of the bar induces a frequency downshift in the spectral peak of the radiated long waves, a consequence of the increased surf zone width on the barred beach and a clear signature of long wave forcing by a time-varying breakpoint. Further comparisons of the two data sets suggest that the bar leads to resonant trapping and amplification (or suppression) of the shoreline motion at discrete long wave frequencies. Well-defined standing long wave motion occurs at discrete frequencies inside the bar and the resonant response is consistent with a simple seiche between the bar crest and shoreline, in agreement with previous numerical model studies. The long wave structure offshore of the breakpoint depends on the relative positions of the bar, shoreline and breakpoint, and is inconsistent with a numerical solution for a free standing long wave over the barred beach profile.

1. Introduction

Many natural beaches have a longshore sand bar, or series of bars, running approximately parallel to the shoreline. In comparison to a plane beach, the bar typically induces wave breaking at specific locations for certain combinations of water depth (tidal level) and wave height. In general, wave breaking leads to a transfer of the incoming short wave energy to a range of different scales of motion, and particularly to lower frequencies (Wright, Guza & Short 1982; Guza & Thornton 1985; and others). These long waves, collectively termed surf beat (Munk 1949; Tucker 1950), may propagate in the cross-shore direction (leaky waves), be refractively trapped (edge waves) or be a mixture of both modes (Huntley, Guza & Thornton 1981; Oltman-Shay & Guza 1987). Since the short wave breaking is strongly influenced by the beach profile, the long wave forcing and resultant motion may be quite different on plane and barred beaches. In addition, the strong correspondence between the length scale of the long waves and nearshore morphological features has suggested that cross-shore standing long waves may generate and maintain longshore bars (e.g. Short 1975; Symonds & Bowen 1984; Wright *et al.* 1986; O'Hare & Huntley 1994). This mechanism requires the presence of a dominant long wave frequency, associated with a resonant response between the morphology and long wave. This

paper considers these issues and presents a detailed analysis of the differences between long wave forcing on a barred beach and a plane beach.

1.1. *Previous work*

Following Munk's (1949) and Tucker's (1950) observations, Longuet-Higgins & Stewart (1962, 1964) showed that short wave groups nonlinearly force a long wave, bound to the short wave groups. Longuet-Higgins & Stewart (1962, 1964) suggested that surf beat was consistent with the release of this bound wave during short wave breaking, with subsequent reflection at the shoreline. Qualitative support for this mechanism comes from some field data (e.g. Guza *et al.* 1984), numerical studies (List 1992), with perhaps more quantitative support from recent laboratory data presented by Janssen, Battjes & van Dongeren (2003). However, release and reflection of the bound long wave implies that surf beat amplitudes should show a close to quadratic dependence on the short wave amplitude (Battjes 1988), whereas the majority of field data shows a roughly linear dependence on short wave amplitude (e.g. Guza & Thornton 1985; Herbers *et al.* 1995; Ruessink 1998).

Symonds, Huntley & Bowen (1982) proposed an alternative mechanism for the generation of surf beat which was directly due to the variability of wave breaking, later expanded on by Schaffer (1993). This model proposes that a time-varying breakpoint position (due to incident wave groupiness) radiates long waves at the group frequency both shorewards and seawards. If the shoreward propagating long waves reflect at the shoreline, then an interference pattern is set-up and the amplitude of the final seaward propagating wave should vary according to the long wave frequency and surf zone width. The peak frequency of the radiated long wave spectrum therefore depends on the breakpoint position, and decreases as the surf zone width increases. In addition, according to the breakpoint forcing model surf beat should show a linear dependence on short wave amplitude.

For discrete long wave frequencies, the cross-shore (partial) standing wave structure resulting from these processes strongly depends on the long wave forcing mechanism and the relative phase between the incident bound waves and outgoing free waves (Baldock *et al.* 2000). The cross-shore nodal structure is quite distinct, even for random wave breaking conditions (Baldock & Huntley 2002). Furthermore, if breakpoint forcing is dominant, the partial standing wave structure close to and seaward of the breakpoint will be quite different from that for a free (standing) long wave originating further offshore. This has implications for the modelling of short waves in the coastal zone and the correlation between long and short wave orbital velocities, which strongly governs net sediment transport directions. For a plane beach, Baldock & Huntley (2002) also found that the relationship between the offshore incident short wave amplitude and the associated long wave amplitude was dependent on both cross-shore location and the particular long wave frequency. Shoreline oscillations (swash) are also often dominated by low frequency oscillations, generated by standing waves and edge waves, or when short waves of varying height reach the shoreline, leading to swash–swash interactions (Mase 1995) and both processes may occur together. However, swash–swash interactions themselves do not appear to generate an additional significant outgoing long wave component (Watson, Barnes & Peregrine 1994).

On a barred beach the standing wave structure will be more complicated due to the increased surf zone width, the varying topography and the relative position of the bar and shoreline at different water levels. In addition, there exists the possibility of the resonant trapping (seiching) of both leaky long waves over the bar (Symonds & Bowen

1984) or edge waves (Kirby, Dalrymple & Liu 1981; Bryan & Bowen 1996). Limited field data provide some support for these hypotheses for edge waves (Sallenger & Holman 1987; Aagaard & Bryan 2003), but, as a result, the data suggest that the long waves in these instances were not generated at that location by either incident wave groups or time-varying breakpoint forcing, but rather had propagated along the coast (e.g. Wright *et al.* 1986). For two-dimensional wave conditions Symonds & Bowen (1984) presented a model illustrating that breakpoint forced free long waves could be trapped by barred topography. For a half wave resonant condition associated with a standing wave elevation anti-node at the bar crest, the long wave amplitude at the shoreline increased in comparison to the amplitude on a plane beach. Conversely, for an elevation node at the bar crest the shoreline amplitude could be suppressed. For the example given, the amplification or damping of the shoreline motion was of the order of 50%.

However, the Symonds & Bowen (1984) model does not appear to have been rigorously tested, particularly for leaky waves, and detailed measurements of the cross-shore structure of standing wave motion over barred topography are also limited. On natural beaches direct identification of shoreline amplification would be very difficult, although it may be possible to distinguish possible significant spectral peaks (or the lack of), provided the shoreline run-up spectra are otherwise generally white at long wave frequencies (Sallenger & Holman 1987; Ruessink, Kleinhans & van den Beukel 1998; Holland & Holman 1999). This may only be the case on mildly sloping dissipative beaches. In addition, it might be argued that significant peaks in the shoreline spectra only indicate resonance if the offshore long wave forcing is white. Furthermore, for field data, there is the added difficulty of distinguishing between cross-shore standing waves and high mode edge waves (e.g. Sallenger & Holman 1987). However, on steeper reflective beaches, both plane and barred, swash spectra may not be white at long wave frequencies (Huntley, Guza & Bowen 1977; Bradshaw 1980; Mase 1988; Baldock & Holmes 1999). In addition, significant spectral peaks at the shoreline do not necessarily imply resonant amplification, since the incident short wave groups may have a dominant frequency (e.g. Sobey & Liang 1986), leading to long wave generation around a particular frequency. Laboratory data for surf beat on a barred beach appear limited to that presented by Janssen *et al.* (2003), but those authors did not seek to determine the cross-shore nodal structure of the long wave motion or if resonant trapping occurred over the bar.

The present paper focuses on these aspects and contrasts two-dimensional long wave forcing (cross-shore motions only) on a plane beach and on a barred beach. Through carefully controlled laboratory experiments essentially identical incident random short wave forcing conditions were used for both beaches, thereby considerably simplifying the identification of any resonant long wave behaviour. The influence of the bar on the generation of seaward propagating long waves is also easily isolated, and found to be consistent with the increased surf zone width. The laboratory study includes measurements of incident and outgoing long waves, the correlation between forced long waves and random short wave groups and the dependence of long wave energy on short wave amplitude. A detailed comparison of the cross-shore structure of the long wave motion on both beaches is also presented. Since a comprehensive summary of two-dimensional surf beat forcing mechanisms is given in Baldock *et al.* (2000) and Baldock & Huntley (2002), a summary of the experimental setup and analysis techniques follows immediately in § 2. Section 3 presents and discusses the experimental data, with final conclusions in § 4.

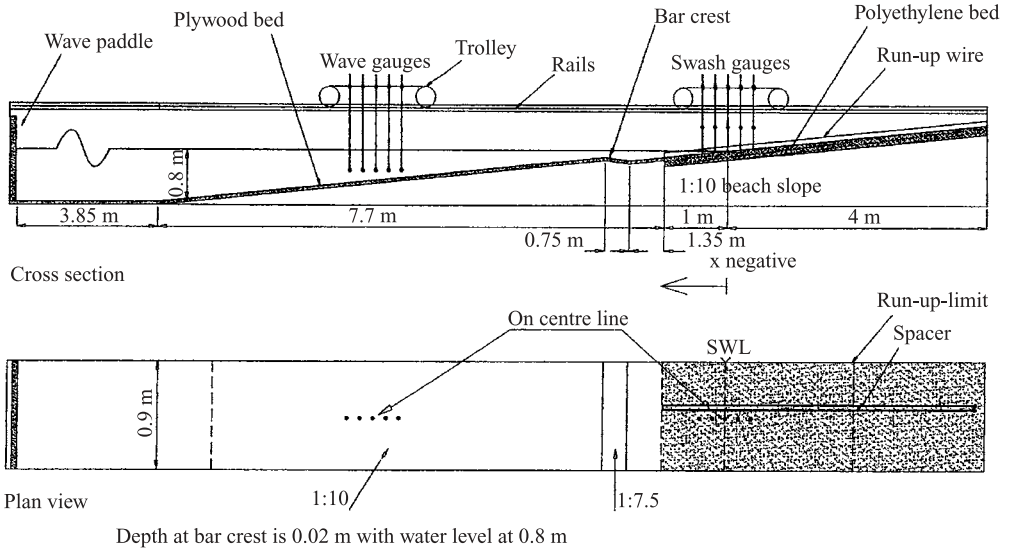

FIGURE 1. Wave flume and instrumentation.

2. Experimental setup

2.1. *Wave flume and instrumentation*

The experiments were carried out in a wave flume 18 m long, 0.9 m wide, with water depths, h, ranging between 0.8 m and 0.86 m (figure 1). Two different beach profiles were utilized in the study. Firstly, a plane beach (gradient $\beta = 0.1$) starting 5.65 m from the wave paddle and, secondly, a barred beach overlying the original plane beach offshore of the bar trough. Offshore of the bar crest and shoreward of the bar trough the beach gradient was maintained at $\beta = 0.1$. The shoreward face of the bar had a gradient of $\beta = 0.16$, with the trough depth, h_t, 0.13 m below the bar crest. The overall beach profile is similar to the universal bar–trough topography described by Wright & Short (1984). For non-breaking monochromatic waves with frequencies of 0.1–0.4 Hz, the reflection coefficient for these beaches ranges from 0.9 to 0.5, with minimal reflection (3–8%) for breaking waves in the frequency range 0.6–1 Hz.

The origin of the horizontal co-ordinate, x, is taken as the intersection of the still water line with the beach face, positive onshore, and is the same for both beach profiles. The location of the bar crest ($x = -2.1$ m) was chosen to coincide approximately with the breaker location for the largest waves on the plane beach, i.e. where a bar might be expected to form naturally. This location also closely coincides with the position of the second anti-node for a free standing long wave with a frequency of approximately 0.2 Hz. On the plane beach, this frequency exhibits maximum surf beat response (maximum outgoing wave amplitude) for the wave conditions used here (Baldock & Huntley 2002). The water depth over the bar crest, h_c, was varied from 0.02 m to 0.08 m, with corresponding distances from the bar to the still water shoreline, X_c, of 2.1 m and 2.7 m.

Waves were generated by a hydraulically driven wedge type wave paddle using second order generation for long waves (Barthel *et al.* 1983). A software driven digital feedback system absorbs up to 60% (in amplitude terms) of waves radiated from the far end of the flume for frequencies at 0.1 Hz, rising to over 90% above 0.4 Hz. The wave motion generated by the wave paddle is highly repeatable, allowing data to be

Series	Case	f_p (Hz)	f_1 (Hz)	f_2 (Hz)	γ	H_{rmso} (m)	ξ	$\overline{h}_b$ (m)
1	J6033A	0.6	0.42	1.47	3.3	0.1	0.61	0.074
1	J6033B	0.6	0.42	1.47	3.3	0.075	0.71	0.055
1	J6033C	0.6	0.42	1.47	3.3	0.05	0.87	0.037
2	J6010A	0.6	0.41	1.48	1.0	0.1	0.61	0.074
2	J6010B	0.6	0.41	1.48	1.0	0.075	0.71	0.055
2	J6010C	0.6	0.41	1.48	1.0	0.05	0.87	0.037
3	J1033C	1.0	0.67	1.78	3.3	0.05	0.56	0.037
3	J1010C	1.0	0.65	1.74	1.0	0.05	0.56	0.037

TABLE 1. Spectral characteristics, Iribarren number and mean breakpoint depth.

collected at multiple cross-shore locations. Data were collected simultaneously from an array of five surface piercing resistance type wave gauges, mounted on a carriage above the flume, and a run-up wire within the swash zone. The absolute accuracy of these wave gauges is of order ± 1 mm, with a resolution better than ± 0.2 mm. The run-up wire consists of two 0.8 mm diameter stainless steel wires 12 mm apart, held 3 mm above the bed, and has a resolution better than ± 0.5 mm in the vertical. Further details of both the wave flume and instrumentation may be found in Baldock *et al.* (2000).

2.2. *Wave characteristics*

The present paper considers data from eight random wave simulations (JONSWAP spectra: Hasselmann *et al.* 1973) with varying peak frequency (f_p), target offshore root mean square wave height (H_{rmso}) and peak enhancement factor, γ. These cases are further subdivided into three series, depending on their peak frequency and spectral shape (table 1). Cases in series 1 have relatively narrow banded frequency spectra ($f_p = 0.6$ Hz, $\gamma = 3.3$, varying H_{rmso}), while those in series 2 are more broad banded ($f_p = 0.6$ Hz, $\gamma = 1$, varying H_{rmso}). Series 3 has cases with both narrow banded and broad banded wave spectra ($f_p = 1$ Hz, $H_{rmso} = 0.05$ m, varying γ). The lower and upper frequency limits for the primary (linear) wave components of the energy spectra, f_1 and f_2 respectively, are also given in table 1, from which long waves frequencies are defined for the purpose of the present study as $f < 0.4$ Hz. The surf similarity parameter, or Iribarren number, $\xi = \beta/\sqrt{(H_{rmso}/L_o)}$, is in the range 0.56–0.87, indicating largely plunging breakers. The majority of the energy dissipation occurs offshore of the bar crest, with approximately 10–15% of the incident short wave energy remaining further shoreward due to the finite water depth over the bar. Consequently, the mean breakpoint position, X, is defined as the location where approximately half this energy (45% of the original offshore wave energy) would be dissipated, i.e. $(H_{rms}/H_{rmso})^2 = 0.55$. The depth at this location, $\overline{h}_b$, may be written as

$$\overline{h}_b = \frac{1}{\kappa}\sqrt{0.55}H_{rmso}, \tag{2.1}$$

where κ is the ratio of the wave height to water depth at breaking. From a series of monochromatic wave measurements, κ has been taken equal to 1, typical of steep beaches, and the resulting values for $\overline{h}_b$ are shown in table 1. Wave breaking was therefore predominantly offshore of the bar crest for h_c=0.02, with breaking on the bar crest and further shoreward for the higher water levels. Values for $\overline{h}_b$ in table 1

are in good agreement with the measured wave heights (e.g. figure 2*a*), suggesting (2.1) provides a reasonable theoretical estimate of the mean breakpoint position.

The same individually generated random wave trains were used for both the plane and barred beach experiments. This allows the influence of the bar on long wave generation to be more easily identified, and also enables direct comparison of the long wave amplitude at the shoreline with and without the bar. In addition, at the wavemaker, the three individually generated random wave trains in each of series 1 and series 2 are identical apart from a change in amplitude. Consequently, any differences in long wave generation due to variations in short wave phase should largely be eliminated when considering the effects of short wave nonlinearity (varying H_{rmso}, see § 3.3). An estimate of the overall surface elevation groupiness, G, is given by (List 1991)

$$G = \frac{\sqrt{2}\sigma_{A(t)}}{\overline{A(t)}}, \tag{2.2}$$

where $\sigma_{A(t)}$ is the standard deviation of the short wave envelope and $A(t)$ is the envelope of the short wave surface elevation. The short wave envelope is readily obtained via a Hilbert transform of the measured surface elevation data (Sobey & Liang 1986). Based on measurements in the constant depth region of the flume, (2.2) gives groupiness values for the random wave cases considered here in the range 0.7–0.8, typical of natural sea states (List 1991).

2.3. *Analysis techniques*

Spectral estimates ($S(f)$) were obtained from Fourier transforms of eight 50 overlapping data segments, each comprising 2048 data points sampled at 25 Hz, with frequency smoothing over three adjacent frequencies (0.0244 Hz). The amplitude, $a(f_c)$, of the long wave motion within finite frequency bands centred on f_c was estimated using the relationship

$$a(f_c) = \sqrt{2\int_{f_c-\delta f}^{f_c+\delta f} S(f)\,\mathrm{d}f}, \tag{2.3}$$

where $\delta f = 0.0122$ Hz and is half the width of the finite frequency band and $S(f)$ is the spectral density of the water surface elevation. Wave heights were estimated from the variance, m_o, of measured surface elevation time-series ($H_{rms}=\sqrt{(8m_o)}$, assuming a narrow-banded Gaussian process and a Rayleigh wave height probability density function, e.g. Massel 1996). Note that each random wave case may be considered to be deterministic, rather than a single realization of random data and therefore the spectra shown later do not require the confidence limits associated with stochastic processes (Baldock, Swan & Taylor 1996). Note that data are only shown from locations seaward of the maximum run-down position and from the run-up wire; consequently time-averaging of the data and spectral calculations were only carried out on continuous data series.

Previous studies (e.g. Guza, Thornton & Holman 1984; Elgar & Guza 1985; List 1992) have used linear theory to separate crudely time-series of incident and outgoing long waves in natural random sea states. Such an analysis ignores the nonlinearity of the incident bound wave, and the influence of the bed slope, which may introduce significant errors, particularly close to the breakpoint. It also assumes that the incident bound wave propagates at the celerity of a free wave, which is only the case if the short waves are shallow water waves. However, a linear analysis is not necessary since incident and outgoing long wave pulses are generally well separated in time, and

may be identified directly through a cross-correlation analysis (Baldock & Huntley 2002; Janssen *et al.* 2003, see § 3.3 below). In addition, the experiments were designed to quantify long wave non-linearity directly and it is therefore also not necessary to decompose the total long wave energy into free and bound long waves by bispectral analysis (e.g. Hasselmann, Munk & Macdonald 1963), which avoids introducing further uncertain spectral estimates.

In order to determine the amplitude of the outgoing free long waves in the constant depth region of the wave flume ($x < -10$ m on the barred beach), calculated second order bound long waves (Longuet-Higgins & Stewart 1960, 1964) were subtracted from Fourier filtered low pass ($f < 0.4$ Hz) measured surface elevation data, theoretically resulting in a surface elevation time series comprising solely of incident and outgoing free long waves (see Baldock & Huntley 2002 for details). The incident and outgoing free long wave surface elevation time series were then separated using the two gauge method of Frigaard & Brorsen (1995), from which both incident and outgoing long wave spectra and amplitudes could be readily determined. The method of Frigaard & Brorsen (1995) was chosen for its simplicity of approach and is applied here in the frequency domain using the full data series. It can also be applied to free waves propagating over sloping bathymetry (Baldock & Simmonds 1999).

The normalized cross-correlation signal, $R_{xy}(\tau)$, between two time series $x(t)$ and $y(t)$ was estimated by (Bendat & Piersol 1986):

$$R_{xy}(\tau) = \frac{\langle x(t)y(t+\tau)\rangle}{\sigma_x \sigma_y}, \tag{2.4}$$

where τ is the time lag between the two signals, σ_x and σ_y are the standard deviations of the respective time series, $\langle\ \rangle$ denotes ensemble averaging and $1 < R_{xy}(\tau) < 1$. In this instance the two time series are the low pass filtered ($f < 0.4$ Hz) long wave surface elevation and the envelope of the short wave surface elevation, $A(t)$, at various cross-shore locations. The normalized cross-correlations were calculated using 4096 data points sampled at 25 Hz, giving for the present data a 95% confidence interval on $R_{xy}(\tau) = 0$ of approximately ± 0.18 (Jenkins & Watts 1968).

3. Discussion of results

3.1. *Offshore spectra and cross-shore wave height variation*

Figure 2 shows examples of the cross-shore variation in wave height (H_{rms}) and steady setup for the three cases in series 1 ($f_p = 0.6$ Hz, $\gamma = 3.3$, varying H_{rmso}). The measured data have been linearly normalized by the target H_{rmso} for each case (see table 1). Hence, in the following, different data sets will overly each other if there is a linear relationship between the data and wave height. The barred beach profile is also shown in figure 2(a), and the bar crest is indicated by the vertical dashed line in figure 2(b). In comparison to the plane beach, the position of the mean breakpoint moves offshore by a distance approximately equal to X_c, the distance between the bar crest and still water shoreline. Figure 2(a) additionally shows that most of the energy dissipation due to wave breaking occurs offshore of the bar crest, with the overall energy dissipation slightly greater than on the plane beach. Steady set-up (figure 2b) reaches a near constant value just shoreward of the bar crest and is linearly dependent on H_{rmso} as expected, with the set-up approaching 20% of the wave height shoreward of the bar crest. The run-up of individual short wave bores elevates the mean shoreline position significantly above the steady set-up in the surf zone, which may be regarded as swash induced set-up as opposed to wave induced set-up. To a first approximation,

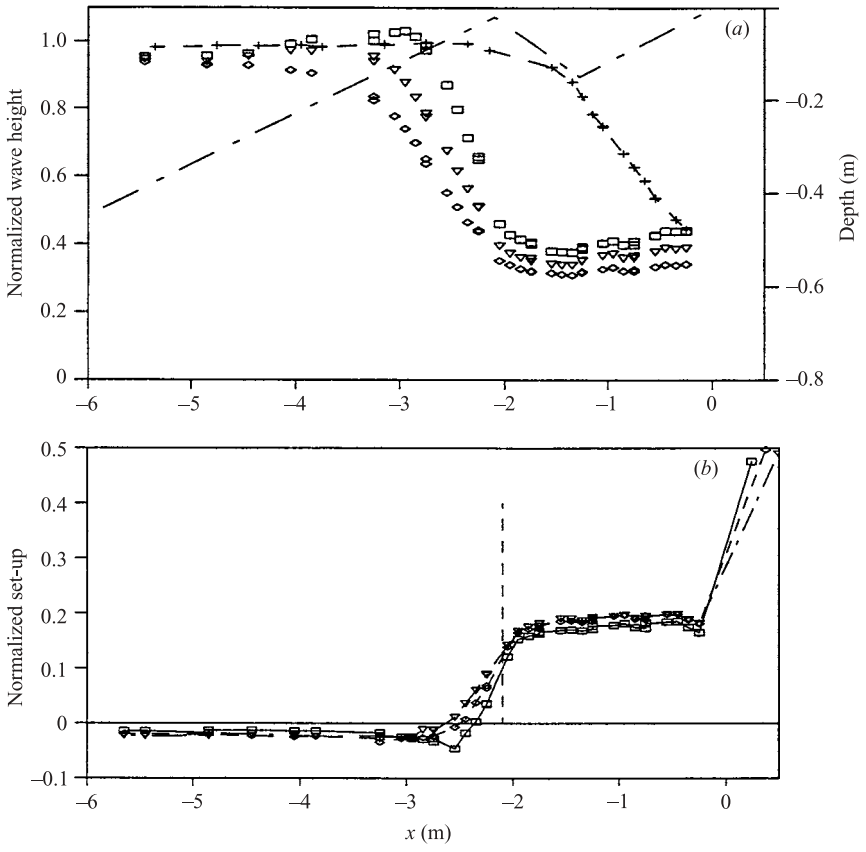

FIGURE 2. (*a*) Cross-shore variation in normalized H_{rms} wave height. (*b*) Cross-shore variation in normalized set-up. Series 1, $\gamma = 3.3$, $h_c = 0.02$ m. ◇, J6033A; ▽, J6033B; □, J6033C; – – + – –, case J6033A, plane beach.

the shoreline motion induced by short wave bores is parabolic (Shen & Meyer 1963), and the mean shoreline is additionally displaced landward by 2/3R, where R is the maximum run-up. R and hence the swash setup may be estimated from the short wave bore height and frequency at the seaward limit of the swash zone (Baldock & Holmes 1999). Using the most shoreward values for H_{rms} shown in figure 2(*a*), the normalized swash set-up for these cases is estimated to be about 0.3, consistent with the data shown in figure 2(*b*).

Surface elevation energy spectra in the constant depth region of the wave flume ($x = -11.15$ m) are shown in figures 3(*a*) and 3(*b*) for cases J6033A (narrow banded) and case J1010C (broad banded), respectively. The measured spectra are in very close agreement with the target first and second order spectra for short wave frequencies ($f > 0.4$ Hz), where the second-order spectra are calculated following Longuet-Higgins & Stewart (1960), see Baldock, Swan & Taylor (1996) for details. However, the measured data show significant additional energy in the long wave frequency band ($f < 0.4$ Hz) and it is shown below that this energy corresponds with long waves propagating offshore. For the plane beach the peak long wave energy occurs at $f \approx 0.2$–0.3 Hz, whereas for the barred beach the additional energy occurs at a much lower frequency, $f \approx 0.05$–0.2 Hz. This frequency downshift in the long

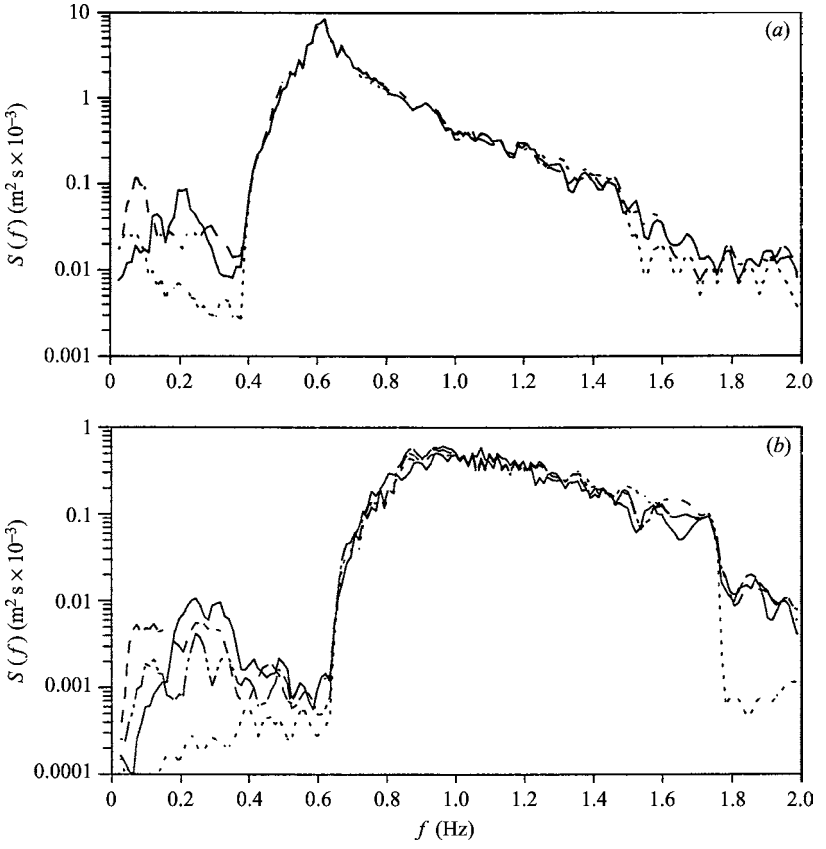

FIGURE 3. Total wave energy spectra at $x = -11.15$ m. (*a*) case J6033A, $H_{rmso} = 0.1$ m. ——, measured (plane beach); – – – –, measured (barred beach); · · · ·, second order solution. (*b*) case J1010C, $H_{rmso} = 0.05$ m. ——, measured (plane beach); – – – –, measured (barred beach, $h_c = 0.02$ m); — · · —, measured (barred beach, $h_c = 0.08$ m); · · · ·, second-order solution.

wave peak frequency is a function of surf zone width, and expected from breakpoint forcing theory (see § 1.1 and § 3.2 below).

A further example of this is illustrated in figure 3(*b*), where, with deeper water over the bar crest ($h_c = 0.08$ m) the main breakpoint moves inshore of the bar and the downshift in the long wave peak frequency is significantly reduced. In fact, for $h_c = 0.08$ m, the long wave energy spectrum becomes quite bi-modal, with two relatively narrow distinct peaks ($f \approx 0.1$ Hz and $f \approx 0.25$ Hz). The latter approximately coincides with the long wave peak frequency on the plane beach. This may be the result of two breakpoints, the first just offshore of the bar crest, with the main breakpoint much closer to the shoreline. Consequently, radiated long waves may be generated at two distinct frequencies. Symonds & Bowen (1984) did not consider this possibility, restricting the forcing region to offshore of the bar.

For all cases shown in figure 3, the computed incident bound wave energy is significantly less than the measured energy at the peak long wave frequency and, particularly for case J1010C, shows little correlation with the data. For case J6033A, the peak bound wave energy and measured long wave energy peak do occur at a similar frequency, $f \approx 0.07$ Hz, but it is shown below that the measured long wave

energy at this location is consistent with breakpoint forced free long waves, rather than released bound waves (see §§ 3.4 and 3.6).

3.2. *Incident and radiated long waves*

On a plane beach, the Symonds *et al.* (1982) forcing model gives an outgoing long wave amplitude that scales according to a non-dimensional measure of the surf zone width given by

$$\chi = \frac{\omega^2 X}{g\beta}, \tag{3.1}$$

where ω is the long wave frequency ($2\pi f$), X is the distance from the mean shoreline to the mean breakpoint position, g is gravitational acceleration and β is the beach slope. For typical surf zone conditions, say $X \approx 80$ m, surf zone gradient $\beta \approx 0.02$ and surf beat periods of order 2 min, then $\chi \approx 1.1$. Symonds *et al.* (1982) show that maximum outgoing long wave generation occurs for $\chi \approx 1.2$, with minimal long wave forcing at $\chi \approx 3.7$. In particular, maximum long wave generation occurs when a standing long wave elevation node coincides closely with the mean breakpoint position. For the plane beach and random wave conditions described above, Baldock & Huntley (2002) found the peak radiated long wave frequency to be $f \approx 0.2$ Hz, corresponding to χ values in the range 1–1.4.

On a barred beach the surf zone width and long wave nodal points depend on the exact topography and long wave frequency. Hence χ becomes less well defined and a less useful measure of the relative position of the long wave nodes and the shoreline. A full numerical solution is used later to determine the nodal positions, and these correlate well with the observed variation in radiated long wave energy. However, a reasonable first estimate of the expected peak radiated long wave frequency can be obtained from (3.1) with $\chi = 1.2$. For case J6033A, $X \approx 3.1$ m and the calculated peak frequency downshifts from $f \approx 0.2$ Hz to $f \approx 0.1$ Hz, for $\beta = 0.1$. It could be argued that β should be representative of the mean beach slope between the shoreline and the breakpoint, in which case the long wave peak frequency would be $f \approx 0.04$ Hz.

Incident and radiated (outgoing) free long waves in the constant depth region of the flume were separated as described in § 2.3. As in Baldock & Huntley (2002) we assume that all outgoing free long waves are generated shoreward of the outer breakpoint by one or more of the mechanisms discussed in § 1, and this is consistent with the data below. Figure 4(*a*) contrasts the incident and radiated free long wave energy spectra obtained from the plane and barred beach for case J6033A. Both data sets show the clear frequency response expected from the breakpoint forcing model, with a clear frequency downshift on the barred beach. The radiated long wave frequency peak is in the range $f \approx 0.06$–0.09 Hz, in close agreement with that estimated above. This frequency downshift in the long wave spectral peak with increased surf zone width appears to be a clear indication of breakpoint forced long waves, and might be useful when analysing data from natural beaches. Figure 4(*b*) shows the ratio of the radiated to incident free long wave amplitude, or radiation coefficient, R_f, again measured in the constant depth region of the flume. Very high radiation coefficients are observed for $0.05 < f < 0.1$ Hz, consistent with free long wave generation further shoreward and confirming the effectiveness of the wave generation and absorption system.

3.3. *Correlation between short waves and long waves*

Figures 5(*a*) and 5(*b*) show the cross-correlation between the short wave envelope in the constant depth region of the flume ($x = -11.15$ m) and the total low frequency

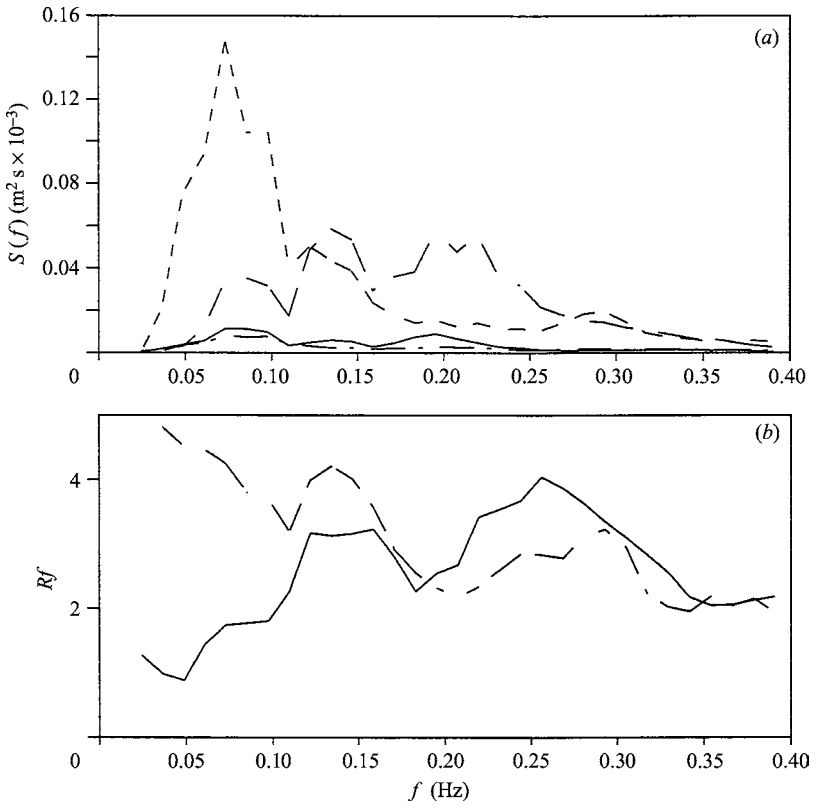

FIGURE 4. (*a*) Incident and radiated free long wave energy spectra at $x = -11.15$ m, case J6033A, $H_{rmso} = 0.1$ m, $h_c = 0.02$ m. ——, Incident (plane beach); —— ——, radiated (plane beach); —·—, incident (barred beach); – – – –, radiated (barred beach). (*b*) Variation in free long wave radiation coefficient with frequency at $x = -11.15$ m. ——, plane beach; – – – –, barred beach.

surface motion ($f < 0.4$ Hz) further shoreward on the barred beach. Figure 5(*a*) shows a strong negative correlation at small lags ($\tau \approx 0$–5 s), with the lag progressively increasing at more shoreward locations. This corresponds to the locally forced incident bound long wave, which is out of phase with the short wave envelope (Longuet-Higgins & Stewart 1962; 1964). The correlation becomes stronger further shoreward as the bound wave shoals and represents a greater proportion of the total long wave energy. A second strong positive correlation is observed at later lags ($\tau \approx 12$–16 s), with the lag reducing for data collected further shoreward. This peak in the correlation signal corresponds to a long wave positively correlated with the incident wave groups and which propagates offshore. Inside the surf zone and in the run-up ($x > -3$ m), the correlation signal shows a single dominant long wave, again positively correlated with the offshore short wave envelope (figure 5*b*). This is to be expected, since larger incident waves will produce a larger dynamic setup. In addition, some wave groupiness persisting inside the bar will continue to generate low frequency motion in the inner surf zone and run-up, which again will be positively correlated with the incident wave groups (Watson & Peregrine 1992).

The positive correlation between the offshore propagating long wave and the incident wave groups is consistent with long waves produced by breakpoint forcing, rather than from the release of the negatively correlated incident bound long wave

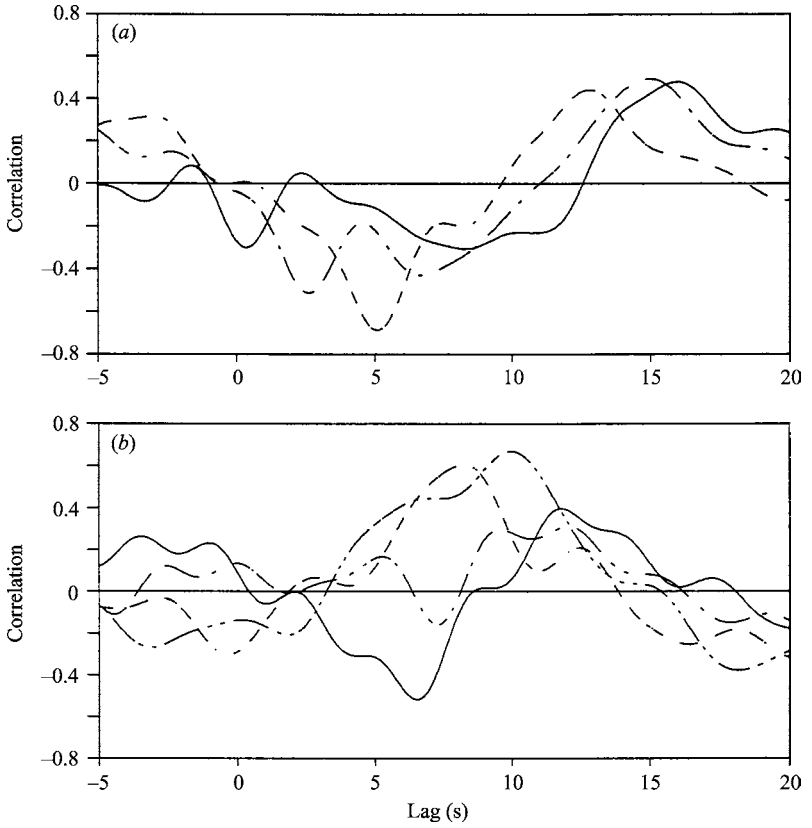

FIGURE 5. Cross-correlation between the wave envelope at $x = -11.15$ and the low frequency motion at more shoreward locations, case J6033A, $H_{rmso} = 0.1$ m, $h_c = 0.02$ m. $x > -3$ m is within the surf zone. (*a*) ——, $x = -11.15$ m; — · —, $x = -8.05$ m; – – – –, $x = -4.85$ m. (*b*) ——, $x = -3.25$ m; — · —, $x = -2.75$ m; — · · —, $x = -1.75$ m; – – – –, run-up.

observed at the outer breakpoint ($x = -3.25$ m, figure 5*b*). These data, together with similar observations from the plane beach by Baldock & Huntley (2002), are in marked contrast to data from a mildly sloping beach presented by Janssen *et al.* (2003) that show an offshore propagating long wave which is negatively correlated with the incident wave groups. This differences appear consistent with the results of Schaffer (1993), who suggests that the shoaling of the incident bound wave reduces with increasing bed slope, and that breakpoint forced waves will become more dominant with increasing wave groupiness inside the surf zone, i.e. on steeper slopes. Battjes *et al.* (2003, in review) draw similar conclusions in a further analysis of the data presented by Janssen *et al.* (2003). It is also relevant to note that most of the extensive field data appropriate for a rigorous examination of the long wave forcing have been obtained from relatively mildly sloping beaches. Future field work on steeper beaches may show results more in accordance with the breakpoint forcing mechanism. Such beaches are widely geographically distributed, particularly in higher latitudes, and often as barrier beaches protecting lower lying coastal regions.

3.4. *Long wave dependence on short wave amplitude and frequency*

Figure 6(*a–f*) shows the cross-shore variation in the total long wave amplitude (incident and reflected, bound and free) within finite frequency bands centred on

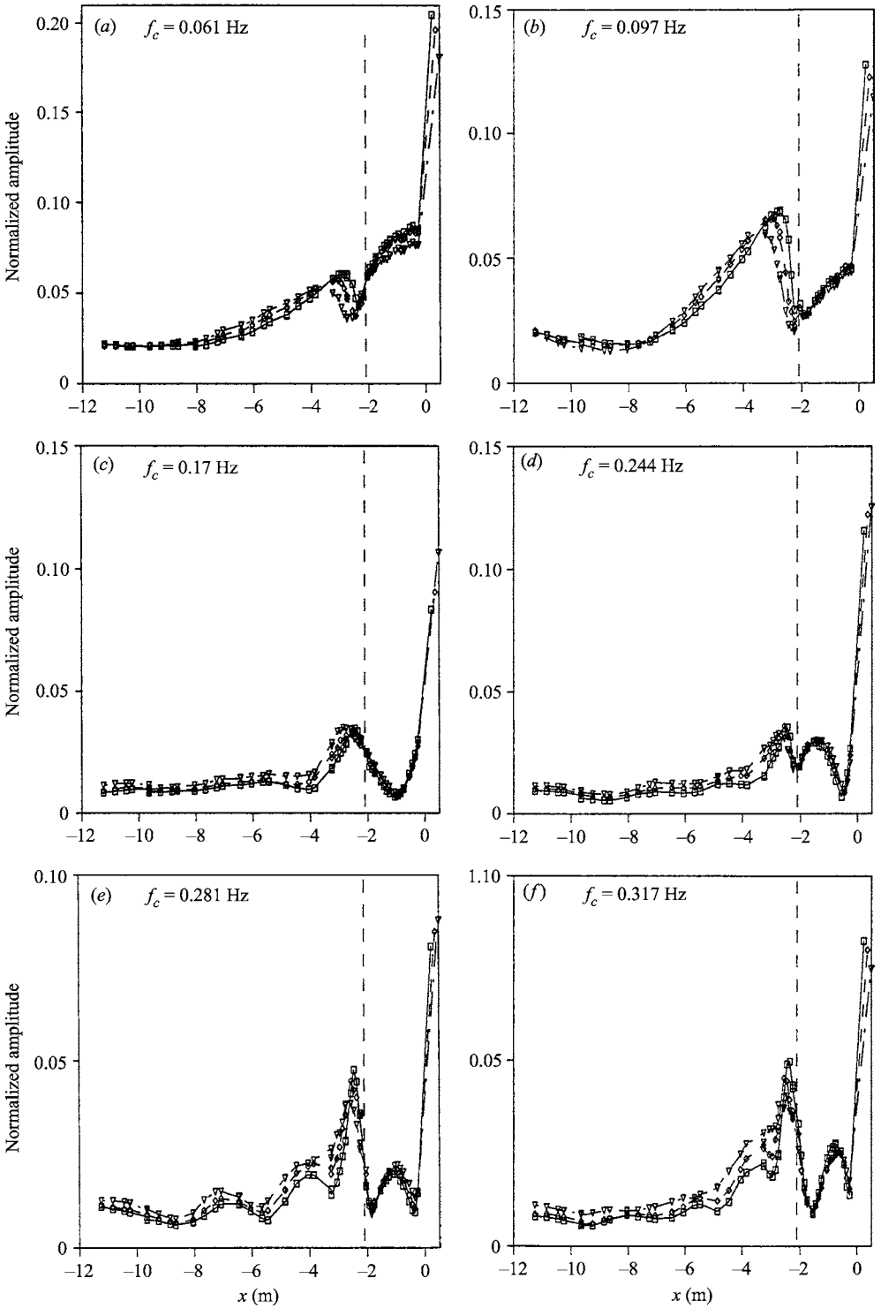

FIGURE 6. Cross-shore variation in normalized wave amplitude at $f_c \pm 0.012$ Hz. Series 1, $\gamma = 3.3$. Vertical line is location of bar crest, $h_c = 0.02$ m. ◇, J6033A; ▽, J6033B; □, J6033C.

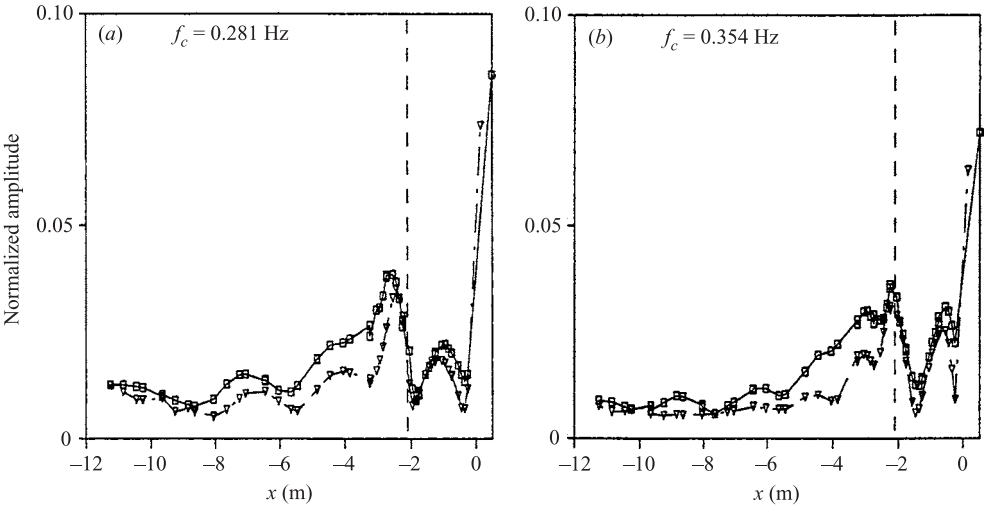

FIGURE 7. Cross-shore variation in normalised wave amplitude at $f_c \pm 0.012$ Hz, Case J6033A ($f_p = 0.6$ Hz, $H_{rmso} = 0.1$ m) and Case J1033C ($f_p = 1$ Hz, $H_{rmso} = 0.05$ m). Vertical line is location of bar crest, $h_c = 0.02$ m. □, J6033A; ▽, J1033C.

f_c (i.e. $f_c \pm 0.012$ Hz). The data are shown for series 1 and have been linearly normalized by the target short wave height, H_{rmso}, for each case. The position of the bar crest is indicated by the vertical dashed line on each figure. At all long wave frequencies ($f < 0.4$ Hz) and at all cross-shore locations the data show a clear linear relationship between short wave height and long wave amplitude, i.e. doubling the short wave height doubles the measured long wave amplitudes. This is consistent with the breakpoint forcing model of Symonds *et al.* (1982), but inconsistent with the release and reflection of a nonlinear bound wave. This is also in agreement with the surface elevation spectra shown in figure 3, where, for the barred beach, the measured long wave energy is significantly greater than the expected bound wave energy over the whole of the long wave frequency range. In contrast, seaward of the breakpoint on the plane beach the bound wave energy dominates the measured energy close to the bound wave spectral peak ($f \approx 0.06$–1 Hz, see figure 3*a*), and the relationship between the long wave amplitude and short wave amplitude is nonlinear at these frequencies (Baldock & Huntley 2002).

The different relationship on the two beaches is a direct consequence of the different surf zone width and the associated frequency downshift in the peak frequency of the breakpoint generated long wave. In general, both the forced and free wave energy are frequency dependent, and each usually show a significant spectral peak. The ratio of forced to free wave long wave energy at any frequency is therefore dependent on the frequency separation of the respective spectral peaks. Consequently, determining the relationship between short wave energy and long wave energy at different frequencies provides additional information on the forcing processes that cannot be obtained by considering the whole long wave spectrum at once (e.g. Herbers *et al.* 1995).

Data for two cases with different short wave height ($H_{rmso} = 0.1$ m and 0.05 m), different short wave peak frequency ($f_p = 0.6$ Hz and 1.0 Hz) and a different wave group time-history (different short wave phasing) are shown in figure 7. For both the frequencies shown the cross-shore structure of the long wave motion is very similar, and is independent of the peak short wave frequency and the precise nature of the

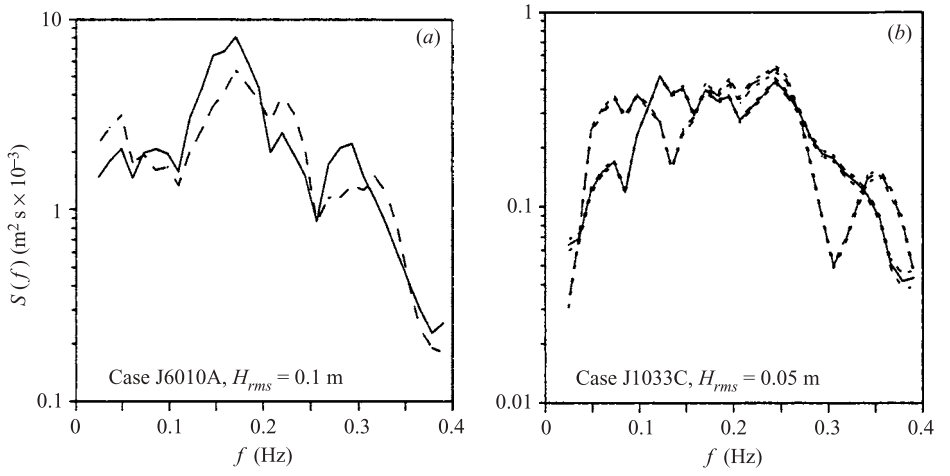

FIGURE 8. Spectral energy in the run-up (swash) on the plane and barred beach. (*a*) Case J6010A, $H_{rms} = 0.1$ m, (*b*) Case J1033C, $H_{rms} = 0.05$ m. ——, plane beach; – – – –, barred beach. Dotted lines on figure 8(*b*) show one standard deviation about the mean spectral energy, based on 12 repeated data runs.

wave grouping. The measured long wave amplitude again scales linearly with short wave height, except in the region of rapid bound wave shoaling prior to breaking where the relationship is weakly nonlinear. This is to be expected, since the shoaling of the incident bound wave is also dependent on the shoaling characteristics of the short waves. In addition the bound wave amplitude will vary with wave groupiness (Symonds *et al.* 1982; Baldock *et al.* 2000), although this seems a relatively constant parameter for natural conditions (List 1991).

3.5. *Shoreline amplitudes*

Two examples of the spectral energy in the run-up (swash) are shown in figure 8(*a*) and 8(*b*) for cases J6010A ($f_p = 0.6$ Hz, broad banded) and J1033C ($f_p = 1$ Hz, narrow banded), respectively. On both the plane and barred beach the run-up spectra are not white in the long wave frequency band, making it difficult to immediately identify any resonant shoreline response for the barred beach. However, subtle differences do occur in the energy spectra, and these are well outside any measurement uncertainties. For example, figure 8(*b*) shows the mean spectral energy, based on twelve repeated runs of the same random wave time series, together with one standard deviation about the mean. The differences between the spectra from the two beach profiles are clearly much greater than likely error bands. Note that a comparison of this form avoids the issue of whether the shoreline spectra, or the offshore forcing spectra, should be white in order to identify resonance, but such an analysis is only possible in the laboratory.

This is further illustrated in figure 9(*a–d*), which shows the ratio of the spectral energy in the run-up on the two beaches (barred beach to plane beach, frequency bands $f_c \pm 0.012$ Hz). Data from four random wave cases are shown, each measured for three different water levels over the bar crest, h_c. Although considerable caution should be taken when taking the ratio of the run-up energy over discrete frequency bands (since small changes in the energy distribution may become magnified), all 12 cases show a very similar pattern. An amplification of order of 50% in the shoreline energy on the barred beach occurs at frequencies $f \approx 0.05$ Hz, 0.2 Hz and 0.35 Hz,

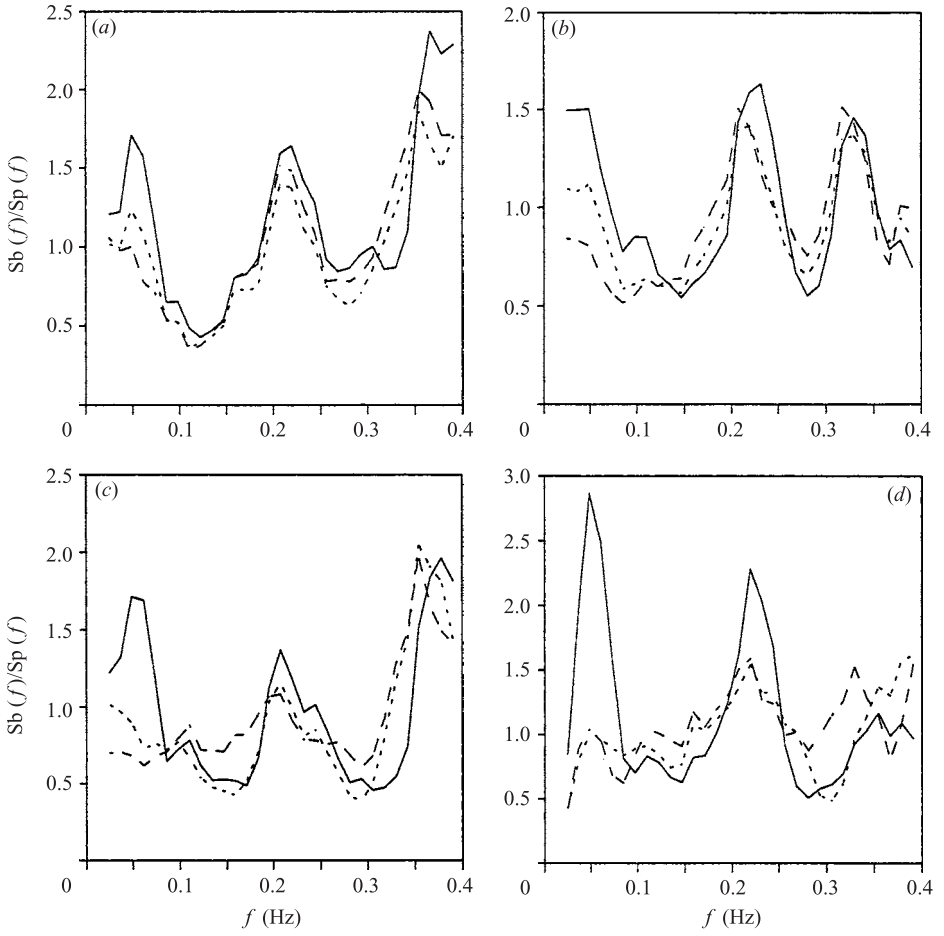

FIGURE 9. Ratio of the spectral energy in the run-up; barred beach to plane beach. (*a*) Case J6033A, $H_{rms} = 0.1$ m. (*b*) Case J6010A, $H_{rms} = 0.1$ m. (*c*) Case J6033C, $H_{rms} = 0.05$ m. (*d*) Case J1010C, $H_{rms} = 0.05$ m. ——, $h_c = 0.02$ m; · · · ·, $h_c = 0.06$ m; – – – –, $h_c = 0.08$ m.

with a similar reduction in energy for $f \approx 0.15$ Hz and 0.3 Hz, and in all cases the degree of amplification is consistent with the model results of Symonds & Bowen (1984).

The frequencies at which resonance might be expected can be estimated numerically from the long wave celerity or from a full numerical solution to the long wave motion over the barred profile (see Symonds & Bowen 1984). However, the resonance condition is a partial seiche between the shoreline and bar crest and, to a first approximation, the simple geometry used here is nearly equivalent to a closed triangular basin with depth $h_t + h_c \approx 0.15$ m. From Dean & Dalrymple (1992), the fundamental frequency of any oscillation and its first harmonic are then estimated to be of order $f = 0.2$ Hz and $f = 0.35$ Hz, in good agreement with the data in figure 9. Furthermore, for the geometry here, an increase in the water depth over the bar would be expected to lead to a lower resonant frequency, and reduced resonance, again consistent with the measured data. In addition, the amplification occurs at frequencies at which the measured and calculated (partial) standing long wave has an elevation anti-node that closely coincides with the bar crest, the half wave resonant

condition identified by Symonds & Bowen (1984). Conversely, the amplification is minimal or the amplitude suppressed if a measured node occurs close to the bar crest (see § 3.6 below).

However, the apparent amplification for $f \approx 0.05$ Hz is not consistent with a seiche mode inside the bar; the first anti-node at this frequency is expected to be far offshore ($x \approx -10$ m, e.g. figure 10*a* below). The shoreline motion at these low frequencies may be influenced by other factors; for example continued long wave forcing inside the bar or swash-swash interactions induced by short wave bores (Watson & Peregrine 1992; Mase 1995; Baldock & Holmes 1999). Both of these are likely to differ on the barred and plane beach. This appears consistent with the general marked reduction in the apparent amplification that is observed for increasing water depths over the bar crest.

3.6. *Cross-shore structure of the long wave motion*

Figure 10(*a–i*) contrasts the cross-shore variation in the total long wave amplitude on the barred beach and plane beach for case J6033A. Again, the data represent the amplitude within finite frequency bands centred on f_c, and the vertical dashed line indicates the position of the bar crest. In addition, the data are compared with a numerical solution for a small amplitude free standing long wave over the barred beach, calculated using a modified form of the shallow water linear long wave model of O'Hare & Huntley (1994). Note, however, that true shallow water conditions ($h/L < 1/20$) are only satisfied for $x > -8$ m at $f \approx 0.2$ Hz and for $x > -5$ m at $f \approx 0.35$ Hz. For each frequency band the model results have been scaled so as to best fit the measured long wave amplitudes inside the bar. The steady setup inside the bar of approximately 0.02 m (figure 2*b*) has been accounted for, fixing the shoreline position in the model at $x = 0.2$ m. Note that direct comparisons cannot be made between the long wave amplitude inside the surf zone on the two beaches due to the different position of nodes and anti-nodes; this can only be carried out for the shoreline amplitudes (figures 8 and 9 above). However, the plane beach data are shown in figure 10 to highlight the change in long wave structure induced by the presence of the bar.

The data show the generation of partial standing waves at discrete frequencies inside the surf zone, with two nodal points inside the bar at higher frequencies ($f > 0.244$ Hz) on the barred beach due to the increased surf zone width. The nodal structure inside the surf zone is also particularly well defined on the barred beach and this increase in the cross-shore variation in amplitude would be beneficial for long wave studies on natural beaches. On the barred beach the nodal and anti-nodal positions are in good agreement with the model predictions inside the breakpoint and the relative sizes of the anti-nodes inside and just outside the bar are also well described by the model (e.g. figures 10 *g–i*). The smaller anti-node inside the bar is due to the deeper water in the bar trough region in comparison to the surf zone depth offshore of the bar crest. However, the model underestimates the shoreline amplitude at the lower frequencies ($f \leqslant 0.17$ Hz). In these cases, short wave swash–swash interactions probably additionally contribute to the magnitude of the measured shoreline amplitudes (e.g. Mase 1995), but there is little evidence of these interactions generating additional outgoing long waves. The maximum shoreline amplification observed at $f \approx 0.2$ Hz and $f \approx 0.35$ Hz (see figure 9) occurs when a long wave surface elevation anti-node occurs at the bar crest (figures 10*e* and 10*i*), in accordance with the Symonds & Bowen (1984) model and the simple seiche condition described above. Minimal amplification or suppression of the shoreline motion occurs when a surface

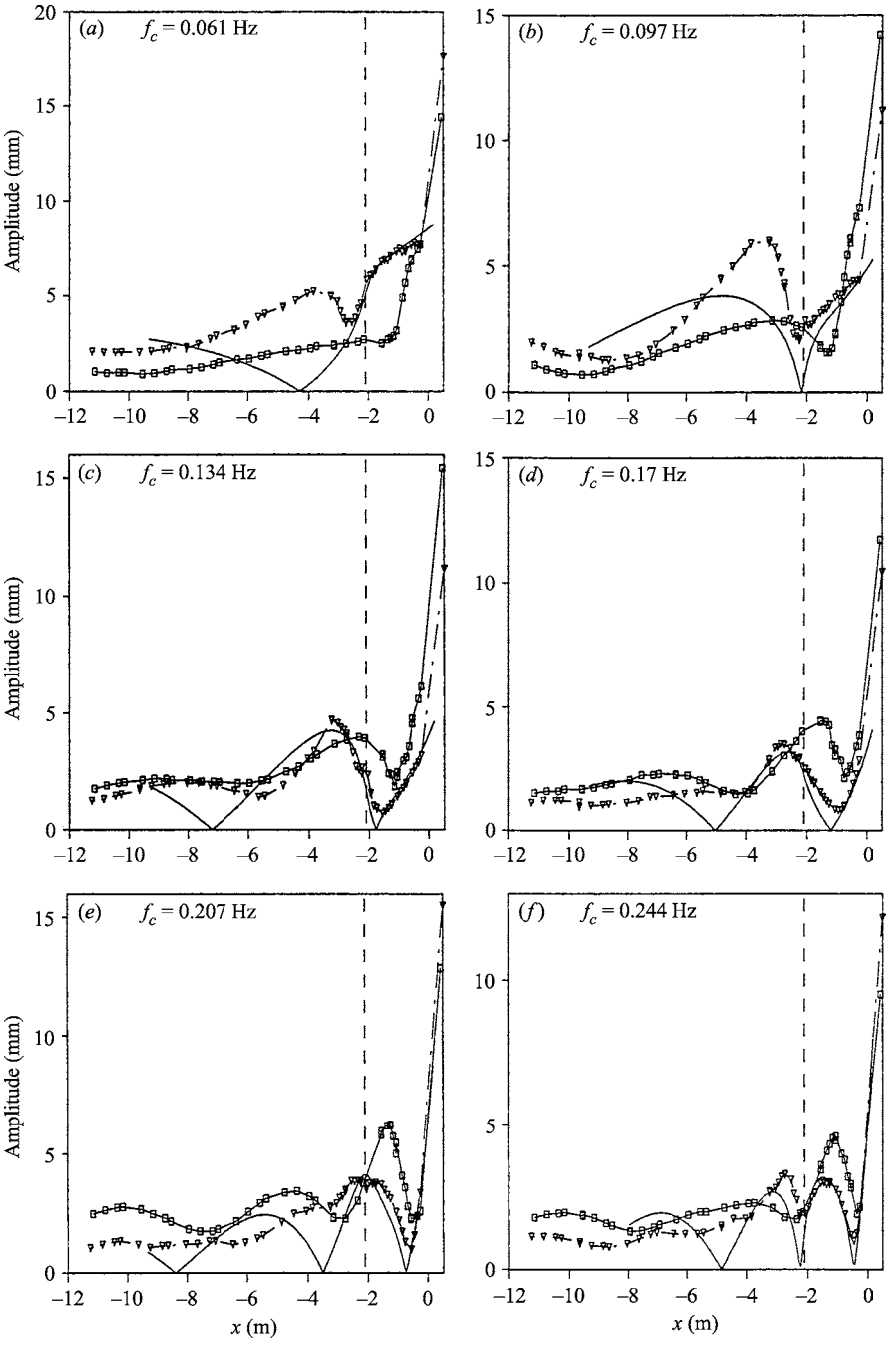

FIGURE 10(*a–f*). For caption see facing page.

elevation node occurs close to the bar crest ($f \approx 0.15$ and $f \approx 0.3$ Hz; figures 10*c* and 10*g*), again consistent with the Symonds & Bowen (1984) results.

Offshore of the breakpoint the data from the barred beach show little correlation with the free standing long wave solution, which is inconsistent with the release and reflection of the incident bound long waves unless a significant phase shift occurs

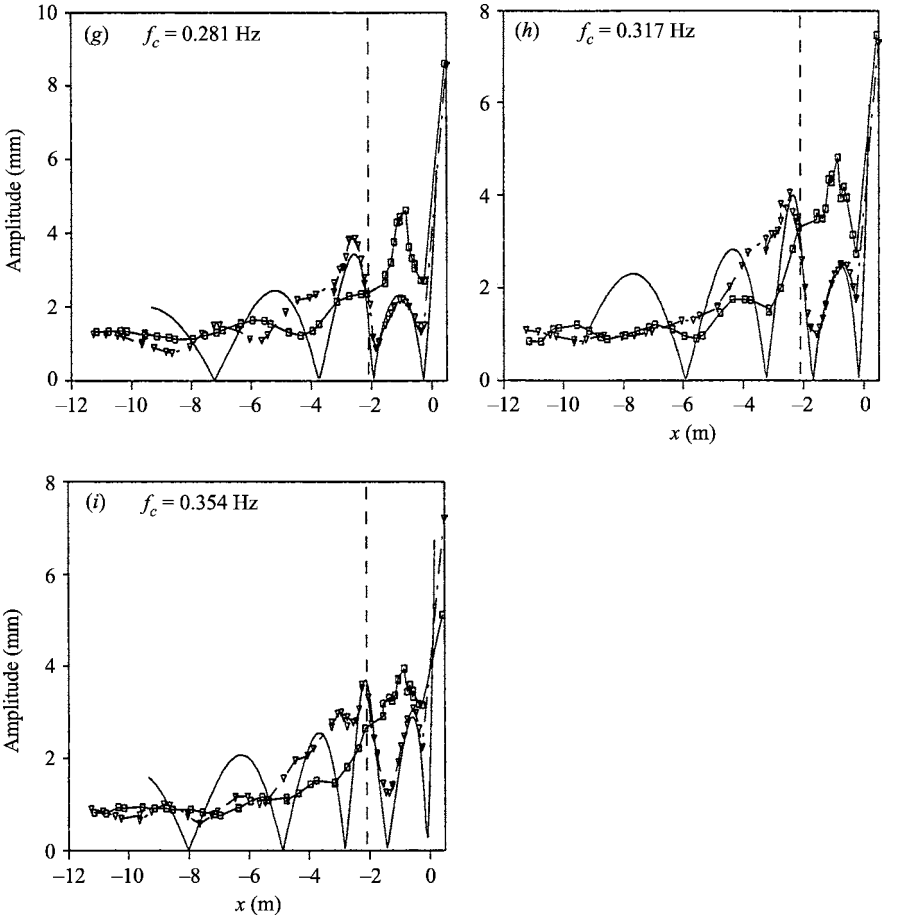

FIGURE 10. Cross-shore variation in wave amplitude at $f_c \pm 0.012$ Hz. Series 1, $\gamma = 3.3$. Vertical line is location of bar crest, $h_c = 0.02$ m. □, plane beach; ▽, barred beach; ——, free standing wave solution (barred beach).

during the propagation of the released long wave through the surf zone (Baldock & Huntley 2002). The nodal structure offshore of the breakpoint results from the interaction of the incident bound long wave and outgoing free long wave, and is therefore also dependent on the relative magnitudes of the two waves. In comparison to the plane beach data, the nodal structure offshore of the breakpoint is much stronger on the barred beach at $f \approx 0.06$–0.13 Hz, but weaker at $f \approx 0.2$–0.28 Hz. This is a further consequence of the frequency downshift in the peak surf beat response on the barred beach, such that, for the wave conditions here, the peak incident bound wave and radiated free wave energy occur at similar frequencies. In contrast, on the plane beach the peak incident and radiated wave energy occur at markedly different frequencies (see figure 2*a*).

It is important to note that an amplification (suppression) of the shoreline motion by resonant trapping does not imply an increase (decrease) in the amplitude of the long wave that is radiated offshore. For example figure 10(*e*) shows a smaller radiated long wave on the barred beach at $f = 0.207$ Hz–0.244 Hz, despite the apparent shoreline amplification, whereas the opposite occurs at $f = 0.097$ Hz (figure 10*b*). This provides

further support for the original breakpoint forcing model of Symonds *et al.* (1982), where the radiated long wave amplitude is dependent on the surf zone width. In this case, a node occurs at the mean breakpoint ($x \approx -2.7$ m, $X \approx 3.1$ m) on the barred beach for $0.061\,\mathrm{Hz} < f < 0.097\,\mathrm{Hz}$ (figures 10*a* and 10*b*), consistent with the peak frequency of the radiated long waves ($f \approx 0.07$ Hz, figure 4*a*). In contrast, for $0.207\,\mathrm{Hz} < f < 0.244\,\mathrm{Hz}$ (figures 10*e* and 10*f*) the mean breakpoint falls between a node and anti-node on the barred beach, resulting in minimal long wave radiation. On the plane beach the mean breakpoint ($x \approx -0.7$ m) coincides with a nodal point for this frequency range, leading to maximum long wave radiation. Outside the surf zone, the radiated long wave characteristics therefore depend on the relative position of both the bar and shoreline and the breakpoint and shoreline. Consequently, the radiated long wave amplitude is dependent on the bar location, the water depth and the wave height. Together with the frequency downshift in the peak frequency of the radiated long waves, such variations might be readily detected on natural beaches.

4. Conclusions

New laboratory data have been presented on long wave forcing by shorter random gravity waves on a barred beach. Eight different random wave simulations have been investigated, covering a range of short wave amplitudes, peak spectral frequency and spectral shape, together with the influence of varying water levels over the bar crest. The distance between the bar crest and the shoreline, and the total surf zone width, therefore also varied. The data include incident and radiated long wave amplitudes, the correlation between short waves and long waves and the detailed cross-shore structure of the long wave motion. The data obtained over the barred beach are critically compared to similar data obtained from a plane beach under essentially identical incident short wave forcing conditions (Baldock & Huntley 2002). The potential for resonant trapping of leaky long waves on a barred beach is investigated (Symonds & Bowen 1984), together with a further comparison of different long wave forcing mechanisms (Longuet-Higgins & Stewart 1962; Symonds *et al.* 1982).

The presence of the bar induces a clear frequency downshift in the spectral peak of the radiated (offshore propagating) long waves. This is a direct result of the increased surf zone width on the barred beach and is consistent with long wave forcing by the time-varying breakpoint induced by incident wave groups (Symonds *et al.* 1982). Maximum long wave radiation occurs when the mean breakpoint closely coincides with a nodal point for a free standing long wave on the barred beach. Bi-modal radiated long wave spectra are observed when short waves break both offshore and shoreward of the bar crest, i.e. when two spatially well separated breakpoints occur.

Outside the surf zone, incident bound long waves are negatively correlated with short wave groups at close to zero lag, as expected from second order wave theory. Strong positive correlations occur at later lags, consistent with an offshore propagating long wave generated by the time-varying breakpoint. On the barred beach, long wave amplitudes are shown to be linearly dependent on the incident short wave amplitude both offshore and shoreward of the breakpoint at all frequencies. This is in contrast to a non-linear dependence at low long wave frequencies on the plane beach (Baldock & Huntley 2002), and is a result of the frequency downshift induced by the bar. The cross-shore variation in long wave amplitude is also shown to be independent of the short wave spectral peak frequency.

A comparison of run-up (swash) spectra obtained from the plane and barred beaches suggests that the presence of the bar leads to resonant trapping of long waves

and amplification (or suppression) of the shoreline motion within finite frequency bands. Amplification (suppression) occurs when the bar crest coincides with an anti-node (node) for a free standing long wave inside the bar-trough surf zone, consistent with the model results of Symonds & Bowen (1984) and a simple seiche between the bar crest and shoreline.

Shoreward of the breakpoint the long wave amplitude and cross-shore structure compare very well with numerical model results for a free standing long wave over the bar- trough profile. Offshore of the breakpoint the data show little correlation with the standing wave solution, again consistent with long wave forcing by a time-varying breakpoint, rather than release and reflection of the incident bound long waves. The long wave structure offshore from the breakpoint depends on the relative position of both the bar and shoreline and the breakpoint and shoreline, and thus will vary with tidal level on natural beaches. Finally, the frequency downshift in the spectral peak of the radiated long waves is clear signature of breakpoint forcing and might be readily detectable on a natural barred beach.

The authors gratefully acknowledge funding from the European Commission, through the MAST III programme, SASME project, Contract no: MAS3-CT97-0081, and additional support from the University of Queensland.

REFERENCES

Aagaard, T. & Bryan, K. R. 2003 Observations of infragravity wave frequency selection. *Continental Shelf Res.* **23**, 1019–1034.

Baldock, T. E. & Holmes, P. 1999 Simulation and prediction of swash oscillations on a steep beach. *Coastal Engng* **36**, 219–242.

Baldock, T. E. & Simmonds, D. 1999 Separation of incident and reflected waves over sloping bathymetry. *Coastal Engng* **38**, 167–176.

Baldock, T. E. & Huntley, D. A. 2002 Long wave forcing by the breaking of random gravity waves on a beach. *Proc. R. Soc. Lond.* A **458**, 2177–2201.

Baldock, T. E., Swan, C. & Taylor, P. H. 1996 A laboratory study of non-linear surface waves on water. *Philos. Trans. R. Soc. Lond.* A **354**, 649–676.

Baldock, T. E., Huntley, D. A., Bird, P. A. D., O'Hare, T. J. & Bullock, G. N. 2000 Breakpoint generated surf beat induced by bichromatic wave groups. *Coastal Engng* **39**, 213–242.

Barthel, V., Mansard, E. P. D., Sand, S. E. & Vis, F. C. 1983 Group-bounded long waves in physical models. *Ocean Engng* **10**, 261–294.

Battjes, J. A. 1988 Surf zone dynamics. *Annu. Rev. Fluid Mech.* **20**, 257–293.

Battjes, J. A., Bakkenes, H. J., Janssen, T. T. & van Dongeren, A. R. 2003 Shoaling of subharmonic gravity waves. *J. Geophys. Res.* (in press).

Bendat, J. S. & Piersol, A. G. 1986 *Random Data, Analysis and Measurement Procedures.* John Wiley.

Bradshaw, M. P. 1980 Topographic control of run-up variability. *Proc. 17th Int. Conf. Coastal Engng*, 1091-1105, ASCE, New York.

Bryan, K. R. & Bowen, A. J. 1996 Edge wave trapping and amplification on barred beaches. *J. Geophys. Res.* **101**, 6543–6552.

Dean, R. G. & Dalrymple, R. A. 1992 *Water Wave Mechanics for Engineers and Scientists.* World Scientific, Singapore.

Elgar, S. & Guza, R. T. 1985 Observations of bispectra of shoaling surface gravity waves. *J. Fluid Mech.* **161**, 425–448.

Frigaard, P. & Brorsen, M. 1995 A time domain method for separating incident and reflected irregular waves. *Coastal Engng* **24**, 205–215.

Guza, R. T. & Thornton, E. B. 1985 Observations of surf beat. *J. Geophys. Res.* **90**, 3162–3172.

Guza, R. T., Thornton, E. B. & Holman, R. A. 1984 Swash on steep and shallow beaches. *Proc. 19th Int. Conf. Coastal Engng*, pp. 708–723. ASCE, New York.

Hasselmann, K., Munk, W. H. & Macdonald, G. 1963 Bispectra of ocean waves. In *Time Series Analysis* (ed. M. Rosenblatt), pp. 125–139. Wiley.

Hasselmann, K., Barnett, T. P., Bouws, E. et al. 1973 Measurements of wind-wave growth and swell decay during the Joint North Sea Wave Project (JONSWAP). Deutches Hydrographisches Institut, Hamburg, Reihe A (8), 12, 95 pp.

Herbers, T. H. C., Elgar, S., Guza, R. T. & O'Reilly, W. C. 1995 Infragravity frequency (0.005–0.05 Hz) motions on the shelf. II. Free waves. *J. Phys. Oceanogr.* **25**, 1063–1079.

Holland, K. T. & Holman, R. A. 1999 Wavenumber-frequency structure of infragravity swash motions. *J. Geophys. Res.* **104**, 13479–13488.

Huntley, D. A., Guza, R. T. & Bowen, A. J. 1977 A universal form for shoreline run-up spectra? *J. Geophys. Res.* **82**, 2577–2581.

Huntley, D. A., Guza, R. T. & Thornton, E. B. 1981 Field observations of surf beat, 1, Progressive edge waves. *J. Geophys. Res.* **86**, 6451–6466.

Janssen, T. T., Battjes, J. A. & Van Dongeren, A. R. 2003 Observations of long waves induced by short wave groups. *J. Geophys. Res.* **108**, 3252–3264.

Jenkins, G. M. & Watts, D. G. 1968 *Spectral Analysis and its Applications.* Holden-Day, San Francisco.

Kirby, J. T., Dalrymple, R. A. & Liu, L. F. 1981 Modification of edge waves by barred beach topography. *Coastal Engng* **5**, 35–49.

List, J. H. 1991 Wave groupiness variations in the nearshore. *Coastal Engng* **15**, 475–496.

List, J. H. 1992 A model for the generation of two dimensional surf beat. *J. Geophys. Res.* **97**, 5623–5635.

Longuet-Higgins, M. S. & Stewart, R. W. 1960 Changes in the form of short gravity waves on long waves and tidal currents. *J. Fluid Mech.* **8**, 565–583.

Longuet-Higgins, M. S. & Stewart, R. W. 1962 Radiation stress and mass transport in gravity waves, with application to 'surf beats'. *J. Fluid Mech.* **13**, 481–504.

Longuet-Higgins, M. S. & Stewart, R. W. 1964 Radiation stress in water waves: a physical discussion with applications. *Deep-Sea Res.* **11**, 529–562.

Mase, H. 1988 Spectral characteristics of random wave run-up. *Coastal Engng* **12**, 175–189.

Mase, H. 1995 Frequency down-shift of swash oscillations compared to incident waves. *J. Hydraulic Res.* **33**, 397–411.

Massel, S. R. 1996 *Ocean Surface Waves: their Physics and Prediction.* World Scientific, Singapore.

Munk, W. H. 1949 Surf beats. *Trans. Am. Geophys. Union* **30**, 849–854.

O'Hare, T. J. & Davies, A. G. 1993 Sand bar evolution beneath partially standing waves: laboratory experiments and model simulations. *Continental Shelf Res.* **13**, 1149–1181.

O'Hare, T. J. & Huntley, D. A. 1994 Bar formation due to wave groups and associated long waves. *Mar. Geol.* **116**, 313–325.

Oltman-Shay, J. & Guza, R. T. 1987 Infragravity edge wave observations on two California beaches. *J. Phys. Oceanogr.* **17**, 644–663.

Ruessink, B. G. 1998 Bound and free infragravity waves in the nearshore zone under breaking and nonbreaking conditions. *J. Geophys. Res.* **103**, 12795–12805.

Ruessink, B. G., Kleinhans, M. G. & van den Beukel, P. G. L. 1998 Observations of swash under highly dissipative conditions. *J. Geophys. Res.* **103**, 3111–3118.

Sallenger, A. H. & Holman, R. A. 1987 Infragravity waves over a natural barred profile. *J. Geophys. Res.* **92**, 9531–9540.

Schaffer, H. A. 1993 Infragravity waves induced by short wave groups. *J. Fluid Mech.* **247**, 551–588.

Shen, M. C. & Meyer, R. E. 1963 Climb of a bore on a beach 3: run-up. *J. Fluid Mech.* **16**, 113–125.

Short, A. D. 1975 Multiple offshore bars and standing waves. *J. Geophys. Res.* **80**, 3838–3840.

Sobey, R. J. & Liang, H.-B. 1986 Complex envelope identification of wave groups. *Proc. 20th Int. Conf. Coastal Engng*, pp. 752–766. ASCE, New York.

Symonds, G. & Bowen, A. J. 1984 Interaction of nearshore bars with incoming wave groups. *J. Geophys. Res.* **89**, 1953–1959.

Symonds, G., Huntley, D. A. & Bowen, A. J. 1982 Two-dimensional surf beat: long wave generation by a time-varying breakpoint. *J. Geophys. Res.* **87**, 492–498.

Tucker, M. J. 1950 Surf beats: sea waves of 1 to 5 min. period. *Proc. R. Soc. Londo.* A **202**, 565–573.

Watson, G. & Peregrine, D. H. 1992 Low frequency waves in the surf zone. *Proc. 23rd Int. Conf. Coastal Engng*, pp. 818–831. ASCE, New York.

Watson, G., Barnes, T. C. D. & Peregrine, D. H. 1994 The generation of low frequency waves by a single wave group incident on a beach. *Proc. 24th Intl Conf. Coastal Engng* ASCE, pp. 776–790.

Wright, L. D. & Short, A. D. 1984 Morphodynamic variability of surf zones and beaches: a synthesis. *Mar. Geol.* **56**, 93–118.

Wright, L. D., Guza, R. T. & Short, A. D. 1982 Dynamics of a high energy dissipative surf zone. *Mar. Geol.* **45**, 41–62.

Wright, L. D., Nielsen, P., Shi, N. C. & List, J. H. 1986 Morphodynamics of a bar-trough surf zone. *Mar. Geol.* **70**, 251–285.